Journal of Solid State Chemistry 198 (2013) 466–474

Contents lists available at SciVerse ScienceDirect

Journal of Solid State Chemistry

journal homepage: www.elsevier.com/locate/jssc

Towards new binary compounds: Synthesis of amorphous phosphorus carbide by pulsed laser deposition

Judy N. Hart [a,*], Paul W. May [a], Neil L. Allan [a], Keith R. Hallam [b], Frederik Claeyssens [c], Gareth M. Fuge [a], Michelle Ruda [a], Peter J. Heard [b]

[a] School of Chemistry, University of Bristol, Bristol BS8 1TS, United Kingdom
[b] Interface Analysis Centre, University of Bristol, 121 St. Michaels Hill, Bristol BS2 8BS, United Kingdom
[c] Kroto Research Institute, Department of Materials Science and Engineering, University of Sheffield, Broad Lane, Sheffield S3 7HQ, United Kingdom

ARTICLE INFO

Article history:
Received 1 June 2012
Received in revised form
6 November 2012
Accepted 11 November 2012
Available online 28 November 2012

Keywords:
Phosphorus carbide
Pulsed laser deposition
X-ray photoelectron spectroscopy

ABSTRACT

We have recently undertaken comprehensive computational studies predicting possible crystal structures of the as yet unknown phosphorus carbide as a function of composition. In this work, we report the synthesis of amorphous phosphorus–carbon films by pulsed laser deposition. The local bonding environments of carbon and phosphorus in the synthesised materials have been analysed by x-ray photoelectron spectroscopy; we have found strong evidence for the formation of direct P–C bonding and hence phosphorus carbide. There is a good agreement between the bonding environments found in this phosphorus carbide material and those predicted in the computational work. In particular, the local bonding environments are consistent with those found in the β-InS-like structures that we predict to be low in energy for phosphorus:carbon ratios between 0.25 and 1.

1. Introduction

There has been much interest in carbon nitride since the prediction that β-C_3N_4 should have a hardness equal to or greater than diamond [1]. However, synthesis of this material has proven to be difficult and success to date has been limited to mixtures of the α- and β-C_3N_4 phases in the form of nanoparticles and nanocrystals embedded in an amorphous network [2–4]. For this reason, in recent work we have used computational approaches to study related materials, including carbon nitrides with a lower nitrogen:carbon ratio [5]. We have also undertaken a detailed computational study of possible crystalline forms of phosphorus carbide [6–9]. By studying structures for a range of compositions, we have been able to predict the preferred local bonding environments of carbon and phosphorus as a function of composition [6]. When the phosphorus content is low, the preferred type of structure is phosphorus-doped graphite (Fig. 1a), in which the carbon is sp^2 hybridised, the phosphorus is two-coordinated and, formally, there are delocalised electrons. However, when the phosphorus content is $\gtrsim 20$ at%, the preferred structures contain sp^2 hybridised carbon and four-coordinated, formally hypervalent phosphorus (Fig. 1b and c). We call structures with these local bonding environments β-InS-like, regardless of stoichiometry, because for the 1:1 stoichiometry the structure with these local bonding environments has the same space group and atoms at the same special positions as the β-InS structure. These structures can also be considered as phosphorus-substituted graphite with P–P bonds between the phosphorus atoms in adjacent layers. In these "pillared" or β-InS-like structures, it is also possible for phosphorus to occupy the three-coordinate sites and carbon the four-coordinate sites, but this is higher in energy than the reverse. Another type of structure considered in the computational studies is pseudocubic-like, in which the carbon is sp^3 hybridised and the phosphorus is three-coordinated (Fig. 1d). Structures of this type generally have a relatively high energy of formation from the pure elements, although they may be the preferred type of structure when the phosphorus content is high (>50 at%) [6]. We are now interested in testing these theoretical predictions of preferred local bonding environments by synthesising phosphorus carbide materials.

Phosphorus-doped carbon and phosphorus carbide films have been previously produced by ion implantation of trimethylphosphine into polyethylene [10], RF plasma CVD [11–13], cathode arc deposition [14], pulsed laser deposition [8] and magnetron sputtering [15]. However, the formation of crystalline phosphorus carbide has not been observed. These experimental reports suggest that the incorporation of small quantities of phosphorus into carbon favours sp^2 hybridised carbon over sp^3 [16,17], consistent with our predictions. Combined experimental and computational studies of fullerene-like phosphorus carbide have

* Corresponding author. Fax: +44 117 927 7985.
E-mail address: Judy.Hart@bristol.ac.uk (J.N. Hart).

0022-4596/$ - see front matter © 2012 Elsevier Inc. All rights reserved.
http://dx.doi.org/10.1016/j.jssc.2012.11.008

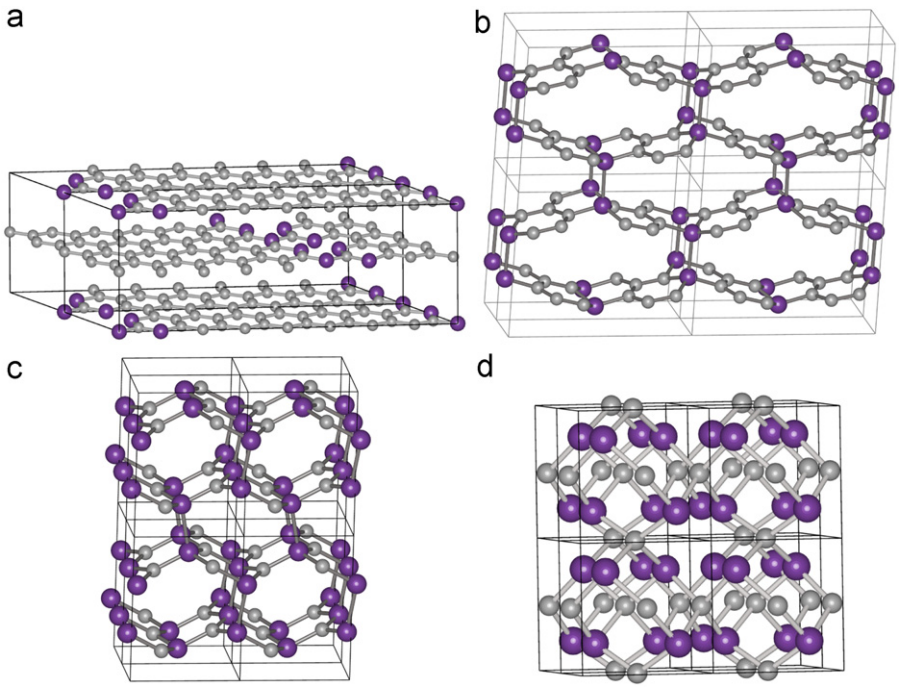

Fig. 1. Preferred structures for different P_xC_y compositions: (a) phosphorus-doped graphite for P_4C_{27}; (b) β-InS-like structure for PC_3; (c) β-InS-like structure for PC; (d) pseudocubic-like structure for P_4C_3. The light grey and the darker purple atoms are carbon and phosphorus, respectively, and the black lines show the unit-cell boundaries. Images of structures were produced with VESTA [21]. (For interpretation of the references to colour in this figure caption, the reader is referred to the web version of this article.)

also been reported previously [15,18–20]; the results indicate that the preferred structures when the phosphorus content is low include highly curved graphene sheets. This is consistent with our prediction that graphite-like structures are usually distorted and buckled, with the phosphorus adopting a pyramidal geometry [6].

These previous experimental reports suggest that phosphorus carbide materials have applications as semiconductors, electrochemical electrodes, electron field emitters and tribological coating materials [13,15–17,20]. It has been found that incorporation of phosphorus in amorphous carbon films significantly increases conductivity, resulting in materials that are promising as electrode materials for electroanalysis [14]. Also, phosphorus carbide thin films have been studied as biocompatible coatings. For example, Kwok et al. [22–24] reported an improved haemocompatiblity of phosphorus-doped diamond-like carbon (DLC) films compared to undoped DLC films. Additionally, the studies of Kelly et al. [25] and Regan et al. [26] indicate that phosphorus-doped DLC thin films exhibit good neurocompatibility and enhanced neuronal adhesion compared to undoped DLC.

2. Experimental methods

Phosphorus–carbon films were deposited on n-type single crystal (100) silicon ($\sim 1\ cm^2$) substrates by pulsed laser deposition. Targets for ablation were produced by pressing a mixture of red phosphorus and graphite powder under a 10 t load to form a disc with a diameter of 16 mm. Targets were made with a phosphorus content up to 37 at%. The target was mounted on a rotating stage in a stainless steel chamber evacuated to $\sim 10^{-6}$ torr. The output of an ArF excimer laser (Lambda-Physik, Compex 201, 193 nm wavelength, 10 Hz repetition rate, ~ 25 ns pulse length) was focused onto the target; the focal spot size on the target was $\sim 1\ mm^2$, giving an incident energy fluence of $\sim 8\ J\ cm^{-2}$ ($\sim 3\times 10^8\ W\ cm^{-2}$). The deposition time was 20 min. The silicon substrate was mounted perpendicular to the target surface normal at a distance of ~ 9 cm from the target. Substrates were heated both during and after film deposition (while still under vacuum in the deposition chamber) by placing a 250 W incandescent light bulb behind the substrate; a thermocouple was attached to the substrate to allow the temperature to be monitored. The films were analysed by scanning electron microscopy (JEOL JSM 5600LV), which showed that they were dense with a smooth, featureless surface. The film thickness was measured by atomic force microscope (Bruker Multimode) imaging over a step in the film created by masking part of the substrate during deposition. The thickness increased as the phosphorus content increased, due to the higher ablation rate of phosphorus compared with carbon [8], and was typically $\sim 30-100$ nm.

X-ray photoelectron spectroscopy (XPS) was used to determine the chemical composition of the outer few nanometres of the deposited films. Areas of $\sim 4\ mm \times 3\ mm$ on each sample were analysed with a Thermo Fisher Scientific Escascope spectrometer, with an Al$K\alpha$ (1486.6 eV) X-ray source operated at 280 W (14 kV, 20 mA). The analyser had a pass energy of 30 eV; the use of a relatively high pass energy was necessary for an adequate count rate. Wide-scan survey spectra were obtained between binding energies of 1000 eV and 0 eV with a step size of 1.0 eV. Subsequent higher energy resolution scans over variable binding energy ranges with 0.1 eV steps were recorded for specific elements of interest (C 1*s*, O 1*s* and P 2*p*). The operating vacuum during analysis was $\sim 5\times 10^{-9}$ mbar.

Fityk version 0.8.6 software was used for peak fitting and quantitative analysis [27]. The relative quantities of carbon, phosphorus and oxygen in the samples were determined from the peak areas, which were weighted by atomic sensitivity factors of 1.00, 2.85 and 1.25 for carbon, oxygen and phosphorus, respectively. All spectra were corrected for charging effects with respect to the carbon 1*s* peak for sp^2 carbon at 284.6 eV [28–30]. To quantify the different bonding environments, the carbon 1*s* and phosphorus 2*p* peaks were fitted with a linear background and a series of pseudo-Voigt functions. A Shirley background was

used initially, but was found to give a poor fit, particularly for the phosphorus 2*p* peaks. For each sample, all pseudo-Voigt functions had the same FWHM and Gaussian:Lorentzian ratio. For phosphorus, pseudo-Voigt functions were used in pairs representing $2p_{3/2}$ and $2p_{1/2}$, with the $2p_{1/2}$ peak at a binding energy 0.84 eV higher than the $2p_{3/2}$ peak and with half the height. Peak positions were unconstrained during fitting, except where the peak intensity was low.

It is known that the carbon 1*s* XPS peak for pure graphite is asymmetric [31]. The fitting was repeated for all samples using an asymmetric peak for sp^2 carbon, but the results were not significantly different, so the results presented are for the symmetric pseudo-Voigt functions, since the calculation of ratio of peak areas is much simpler in this case.

SIMS spectra were obtained using an electronically variable aperture type gallium ion gun (FEI SD gallium LMIS EVA focusing column) fitted to a double-focusing magnetic sector mass analyser (Vacuum Generators model 7035). The system vacuum during operation was 10^{-7} mbar. The instrument was calibrated using a value of 68.93 for the backscattered Ga^+ ions. SIMS surface spectra were obtained by scanning a 3 nA, 25 keV gallium ion beam over an area of 400 μm × 400 μm while scanning the magnet to accept secondary ions in the range 0–100 Da, with a step size of 0.05 Da and a dwell time of 100 ms per step. Dynamic depth profiles were obtained by continual secondary ion analysis whilst etching through the sample layer, scanning the ion beam over an area of 130 μm × 130 μm. A gating facility was used to restrict ion counting to the centre of the etch pit in order to avoid edge effects.

The films were also analysed by laser Raman spectroscopy using a Renishaw 2000 system with an excitation wavelength of 514.5 nm.

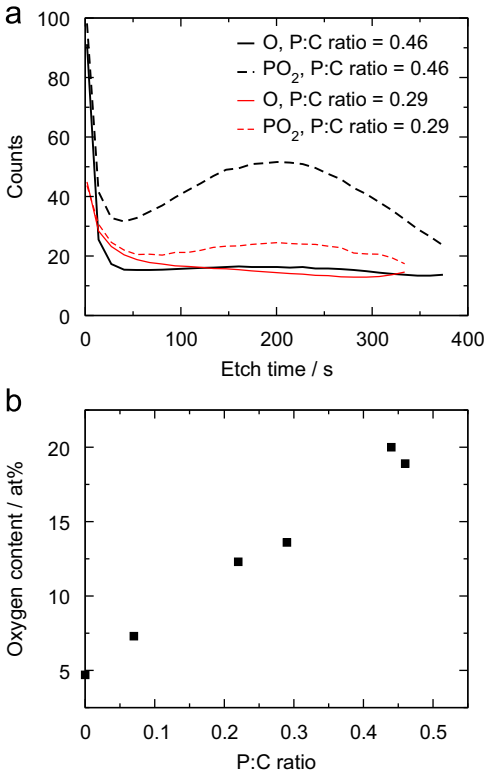

Fig. 2. (a) SIMS depth profiles for oxygen and PO_2 for films with two different compositions. (b) Oxygen content as a function of phosphorus content, measured by XPS.

3. Results and discussion

3.1. Composition

The phosphorus:carbon atomic ratio and oxygen content of the deposited films, measured by XPS, are shown in Table 1. Throughout this paper, the composition of the deposited films is referred to in terms of the P:C atomic ratio measured by XPS. Targets with the same composition can lead to films with different compositions measured by XPS, probably due to local variations in the composition of the films and non-uniformity in the composition of the targets. Both SIMS and XPS indicate that the amount of impurities other than oxygen is low. For example, the nitrogen content is $\lesssim 2$ at%. The amount of OH, CO and CO_2 detected by SIMS is very small, while XPS indicates that $\sim 10\%$ of the carbon is bonded to oxygen.

SIMS depth profiles suggest that the oxygen content is highest near the surface of the films (Fig. 2a), suggesting that the oxygen is adsorbed at the surface after deposition due to exposure to air, although more oxygen is detected through the bulk of the material when the phosphorus content is high.

Table 1
P:C atomic ratio and oxygen content of the deposited films measured by XPS.

Target phosphorus content		P:C atomic ratio	Oxygen content (at%)
at%	P:C atomic ratio		
0	0	–	4.7
4.1	0.04	0.07	7.3
14	0.16	0.22	12.3
28	0.39	0.29	13.6
28	0.39	0.44	20.0
37	0.59	0.46	18.9

Both XPS and SIMS suggest that the oxygen in the deposited films is attached predominantly to phosphorus rather than carbon, consistent with the results of Gorham et al. [10]. XPS results show an increase in the oxygen content as the phosphorus content increases (Table 1 and Fig. 2b), while SIMS results indicate that $\sim 35-50\%$ of the phosphorus is detected as P_xO_y species (mainly PO_2) but $<1\%$ of the carbon is detected in the form of C_xO_y species.

SIMS results suggest the presence of P_xC_y species and hence phosphorus carbide formation. For example, for the two samples with a P:C ratio (measured by XPS) of ~ 0.45, $\sim 25\%$ of the carbon near the surface and $\sim 50\%$ of the phosphorus was detected in the form of P_xC_y species (*e.g.* PC, PC_2, PC_3). The remainder of the carbon was detected in the form of pure carbon species (*e.g.* C, C_2, C_4) and hydrocarbons (*e.g.* CH, C_2H, C_2H_2), while the remainder of the phosphorus was detected in the form of pure phosphorus species and phosphorus oxides (*e.g.* PO_2, PO). A typical SIMS spectrum is shown in the Supplementary Information.

3.2. Raman spectroscopy

The laser Raman spectra for films with no or only a small amount of phosphorus show a strong peak at $\sim 1550\ cm^{-1}$ (Fig. 3). This peak is composed of the sp^2 carbon D and G signals, attributed to the breathing mode of sp^2 carbon rings and the sp^2 carbon stretching mode, respectively [32]. As the phosphorus content increases, this peak becomes weaker and shifts to a lower wavenumber, consistent with previous reports [8,13,14]. It is likely that this wavenumber shift is due to the intensity of the G component decreasing relative to the D component. This could be due to either an increase in the sp^2:sp^3 carbon ratio [8,14] or increasing disorder in graphite-like regions of the films with increasing phosphorus content [32]. The overall weakening of the peak is consistent with the presence of phosphorus disrupting

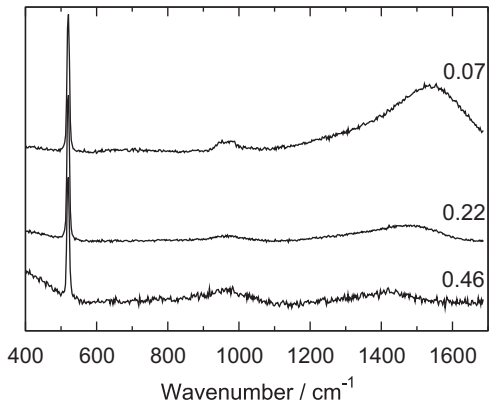

Fig. 3. Raman spectra of phosphorus–carbon films for different values of P:C ratio. Peaks at $\sim 520\ cm^{-1}$ and $\sim 950\ cm^{-1}$ are due to the silicon substrate.

the carbon bonding structures. There are no peaks in the Raman spectra that can be attributed to phosphorus carbide structures; however, Raman peaks for phosphorus carbide are expected to be weak in comparison with the strong sp^2 carbon peak.

3.3. X-Ray photoelectron spectroscopy

3.3.1. Phosphorus

The phosphorus 2*p* peak in the XPS spectra can be seen to be composed of two strong peaks at $\sim 129.6 \pm 0.4$ eV and $\sim 132.5 \pm 0.3$ eV (positions are stated for the $2p_{3/2}$ component, Fig. 4); we assign these peaks to phosphorus–phosphorus bonds and phosphorus–oxygen bonds, respectively.

When fitting the XPS peak to quantify the proportion of phosphorus involved in these two different bonding environments, it was found that including additional peaks at $\sim 131.3 \pm 0.4$ eV and $\sim 133.7 \pm 0.3$ eV significantly improved the fit. These additional peaks were included for all samples. In most cases, their positions were not constrained during fitting and they were found at approximately the same binding energy; however, in cases where the peaks were weak, it was sometimes necessary to constrain the peak position. We tentatively assign these two peaks to phosphorus–carbon bonds. Examples of fitting for the phosphorus 2*p* peak are shown in Fig. 4.

Our value for the P–P binding energy is in good agreement with previous reports for pure phosphorus [33,34]. Furlan et al. [15] also assigned a peak with a $2p_{3/2}$ component at ~ 132.6 eV to P–O bonds for phosphorus carbide films deposited by magnetron sputtering. Gorham et al. [10] similarly assigned peaks at ~ 131 eV and ~ 133 eV in the P 2*p* XPS spectra of phosphorus carbide films formed by ion implantation to P–C bonds and P–O bonds, respectively, while Liu et al. [14,17] assigned an XPS peak at 131.3 ± 0.2 eV to P–C bonds and a peak at 133.3 ± 0.2 eV to P–O bonds.[1] Furlan et al. [15] assigned a peak with a $2p_{3/2}$ component at ~ 130.2 eV to P–C bonds, intermediate between our values for P–P and P–C bonds. However, Furlan et al. neglected the possibility of P–P bonds in the films; if P–P bonds were in fact present, the true P–C binding energy would be higher than the reported value. In addition, different film deposition techniques are likely to give slightly different bonding environments, which may account for the small differences in binding energies.

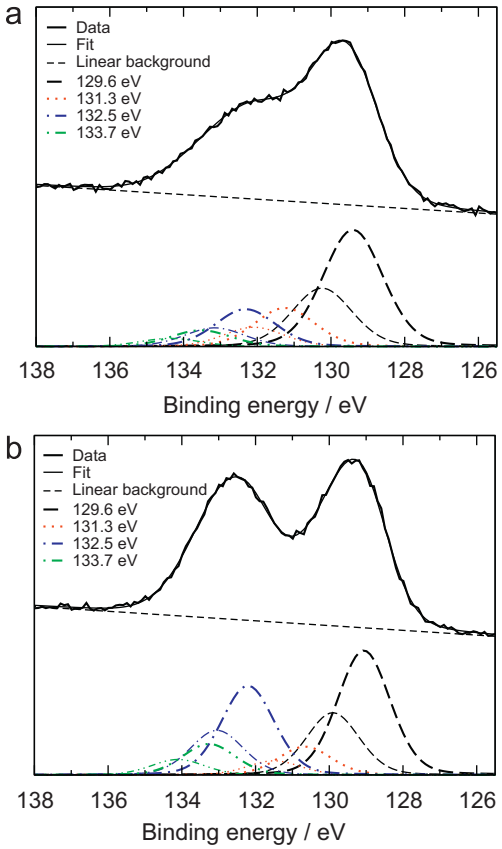

Fig. 4. Examples of curve fitting for the phosphorus 2*p* XPS peak for films with a (a) P:C ratio of 0.22 and (b) P:C ratio of 0.46. Two pseudo-Voigt functions are used for each phosphorus environment, representing $2p_{3/2}$ (bold line) and $2p_{1/2}$. Energies are given for the $2p_{3/2}$ component.

From the computational results, it is possible to predict the relative positions of XPS peaks associated with P–C bonding in different environments to aid the interpretation of the experimental results. This is done by calculating the carbon 1*s* and phosphorus 2*p* orbital energies for graphite and red phosphorus and also for various phosphorus carbide structures. These calculations were carried out with the CRYSTAL code [35–37], using the B3LYP hybrid method [38,39] and previously published basis sets [40–44].[2] The orbital energies were calculated after a full geometry optimisation of all atomic positions and lattice parameters, with the structures constrained to the relevant space group. The equilibrium structure was determined by using a quasi-Newton algorithm with a BFGS Hessian updating scheme. The geometry optimisation convergence was determined from both the root-mean-square (rms) and absolute values of the largest component of the gradients and nuclear displacements. For all atoms, the thresholds for the maximum and rms forces were 0.00045 au and 0.00030 au and those for the maximum and rms atomic displacements were 0.00180 au and 0.00120 au, respectively.

The calculated energies of the phosphorus 2*p* orbitals for red phosphorus and various phosphorus carbide structures are shown schematically in Fig. 5. Phosphorus carbide structures included are β-InS-like structures with hypervalent phosphorus (for PC_3, PC and P_3C_4), β-InS-like structures with three-coordinate

[1] Gorham et al. [10] and Liu et al. [14,17] used only a single peak for phosphorus 2*p* in fitting their XPS spectra, rather than using two peaks corresponding to $2p_{3/2}$ and $2p_{1/2}$. In order to compare our results with these previous reports, we have repeated the fitting using only a single peak for phosphorus 2*p*. In this case, we obtain binding energies of 131.4 ± 0.3 eV for the first P–C peak and 132.8 ± 0.3 eV for P–O.

[2] The calculations of orbital energies for a representative subset of structures were repeated with the PBE0 hybrid method [45]; all results for relative energies were consistent with the results from the calculations using the B3LYP method.

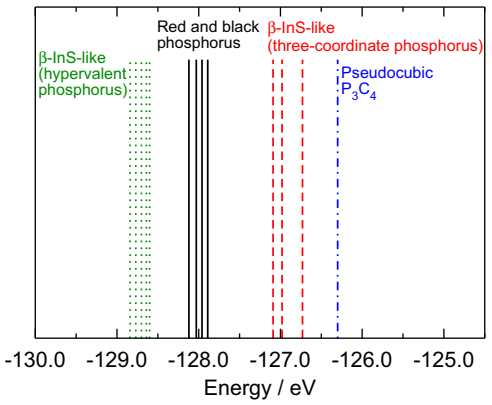

Fig. 5. Calculated phosphorus 2*p* orbital energies for red and black phosphorus and various phosphorus carbide structures.

phosphorus (for PC_3 and PC) and pseudocubic-like P_4C_3 (three-coordinate phosphorus).

It can be seen that for phosphorus in a hypervalent, four-coordinated bonding environment, such as that found in *β*-InS-like structures of phosphorus carbide, an XPS signal would be expected at a binding energy higher than that of pure phosphorus (Fig. 5). For phosphorus in a three-coordinated environment in either *β*-InS-like or pseudocubic-like structures, the phosphorus 2*p* orbital energy is above that for pure phosphorus. The number of structures included in Fig. 5 is limited for clarity; however, the results for other structures are consistent with those shown. For example, a phosphorus-doped graphite structure for P_4C_{11} optimises to a very distorted structure in which there are two-, three- and four-coordinated phosphorus atoms. For the two- and three-coordinated phosphorus atoms, the phosphorus 2*p* orbital energy is between −127.9 eV and −126.5 eV, depending on the exact environment, with a higher coordination generally corresponding to a lower energy. For the phosphorus in an environment with four neighbours (three carbon and one phosphorus), the 2*p* orbital energy is lower (−128.2 eV); however, it is still significantly higher than for phosphorus in the *β*-InS-like structures, in which the P–P bond length is shorter. Hence, four-coordination appears to be the environment that gives a 2*p* orbital energy consistent with the XPS results. For a structure in which all atoms are three-coordinated (*e.g.* the bct4 structure investigated in the computational study [6]) the phosphorus 2*p* orbital energy is calculated to be moderately low (−128.3 eV). However, the carbon 1*s* orbital energy is high (−276.9 eV), which is not consistent with the XPS results for carbon (as discussed below), and structures with this bonding arrangement are high in energy, so are unlikely to be formed. Note that quantitative agreement between the experimental binding energies and computational orbital energies is not expected; it is only relative values of energy that are significant.

3.3.2. Carbon

For samples containing no phosphorus, only a single peak for carbon 1*s* is observed in the XPS spectra (Fig. 6), assumed to be due predominantly to carbon–carbon bonds. When a small amount of phosphorus is included, a second peak appears in the XPS spectrum at ~288.6 eV and this peak becomes stronger as the phosphorus content increases to a P:C ratio of 0.22. When the P:C ratio increases further to 0.46, the intensity of this peak at ~288.6 eV decreases and another peak appears at ~292.6 eV. Since these peaks only appear when phosphorus is present, they are likely to be associated with bonding environments found in phosphorus carbide structures.

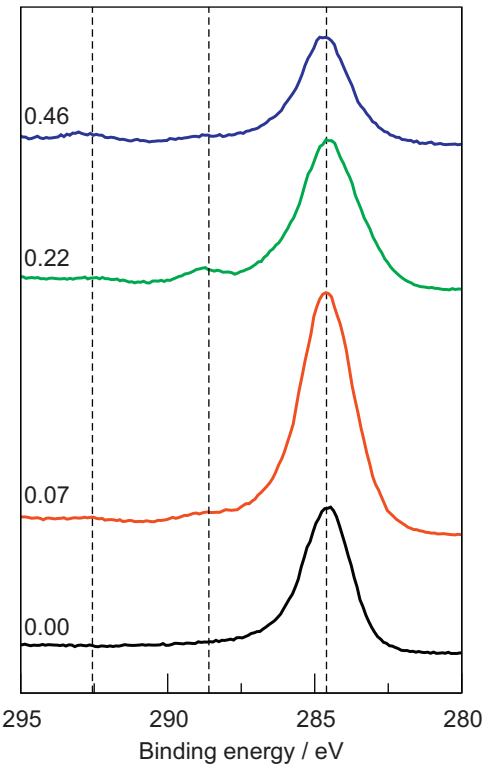

Fig. 6. Carbon 1*s* XPS spectra for different values of P:C ratio. The vertical dotted lines show the positions of the sp^2 carbon peak at 284.6 eV and the two peaks that appear when phosphorus is included at ~288.6 eV and ~292.6 eV. (P:C ratio is the atomic ratio measured by XPS.)

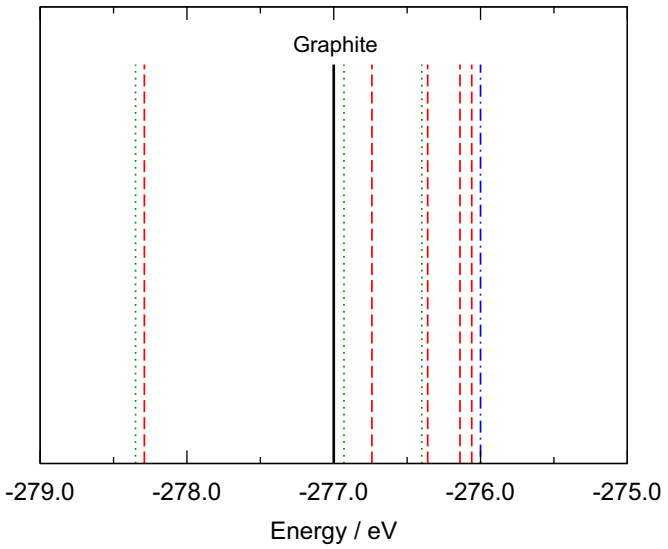

Fig. 7. Calculated carbon 1*s* orbital energies for various *β*-InS-like structures (green dotted lines: PC_3; red dashed lines: P_3C_4; blue dash-dotted line: PC) and graphite (black solid line). (For interpretation of the references to colour in this figure caption, the reader is referred to the web version of this article.)

The calculated carbon 1*s* orbital energies for the *β*-InS-like structures that contain hypervalent phosphorus indicate that a peak would be expected in the XPS spectra for these structures at a binding energy higher than that of carbon in graphite (Fig. 7), consistent with the experimental observation. The carbon atoms with this orbital energy (shown in green in Fig. 8) are bonded only to other carbon atoms, but the orbital energy is modified relative to that of carbon in graphite by the presence of

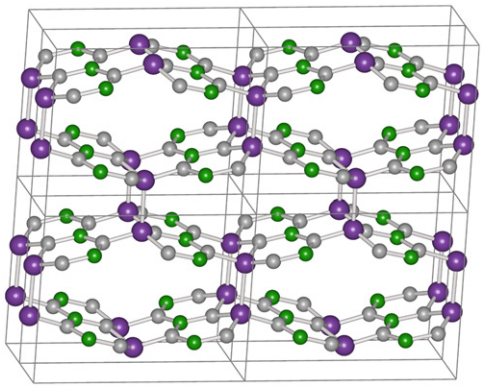

Fig. 8. β-InS-like structure for PC_3. The green and light grey atoms are carbon and the darker purple atoms are phosphorus, and the black lines show the unit-cell boundaries. The carbon 1*s* orbital energy for the green atoms is ~ -278.3 eV, while the remaining carbon atoms have a 1*s* orbital energy between -277.0 eV and -276.3 eV. (For interpretation of the references to colour in this figure caption, the reader is referred to the web version of this article.)

nearby phosphorus atoms. (The calculated carbon 1*s* orbital energies for other phosphorus carbide structures are not consistent with the experimental observation of an XPS peak at a higher binding energy than graphite.) Furthermore, for these β-InS-like structures, another peak would be expected in the carbon 1*s* XPS spectrum, at a lower binding energy than that for graphitic carbon (Fig. 7). This orbital energy is associated with carbon atoms that are bonded directly to hypervalent phosphorus (Fig. 8).

Therefore, the carbon 1*s* XPS peak was fitted with five pseudo-Voigt functions—one for sp^2 hybridised carbon (at ~ 284.6 eV), one for carbon bonded to oxygen (at ~ 286.4 eV), one for each of the two peaks that appear at high binding energies when phosphorus is incorporated (at ~ 288.6 eV and ~ 292.6 eV) plus one for the peak that, based on computational results, is expected to appear at a binding energy lower than that of sp^2 hybridised carbon for β-InS-like structures. Examples of the peak fitting of the carbon 1*s* peak are shown in Fig. 9. As for fitting the phosphorus 2*p* peak, in almost all cases the peak positions were not constrained; a good fit was obtained with this set of peaks for all samples and the peak positions were consistent across all samples to within ~ 0.3 eV. The binding energy for carbon bonded to oxygen found here (~ 286.4 eV) is consistent with that reported by Mérel et al. (~ 286.5 eV) [28]. The binding energy of the peak that is expected for the β-InS-like structures at a binding energy lower than that of sp^2 hybridised carbon is 283.3 ± 0.2 eV.

Only one peak was included for carbon–carbon bonds, rather than one for sp^2 and one for sp^3 hybridised carbon, because of the already high number of fitting parameters. The Raman spectra indicate the presence of sp^2 hybridised carbon and, possibly, that the sp^2:sp^3 carbon ratio increases with phosphorus content. Therefore, it was assumed that the majority of the carbon in the films is sp^2 hybridised and the binding energy of the peak attributed to carbon–carbon bonding in the fitted XPS spectra was set to 284.6 eV. However, it is not possible to rule out the presence of sp^3 hybridised carbon, particularly in the films with low phosphorus content. If sp^3 hybridised carbon is present in a significant quantity, the assumption that the binding energy of the peak attributed to carbon–carbon bonding should be 284.6 eV will lead to a small underestimation of the binding energies of the other peaks.

3.3.3. Correlation between phosphorus and carbon XPS peaks

By measuring the area under the pseudo-Voigt functions, the proportion of carbon and phosphorus in the different bonding environments can be quantified. The proportion of carbon

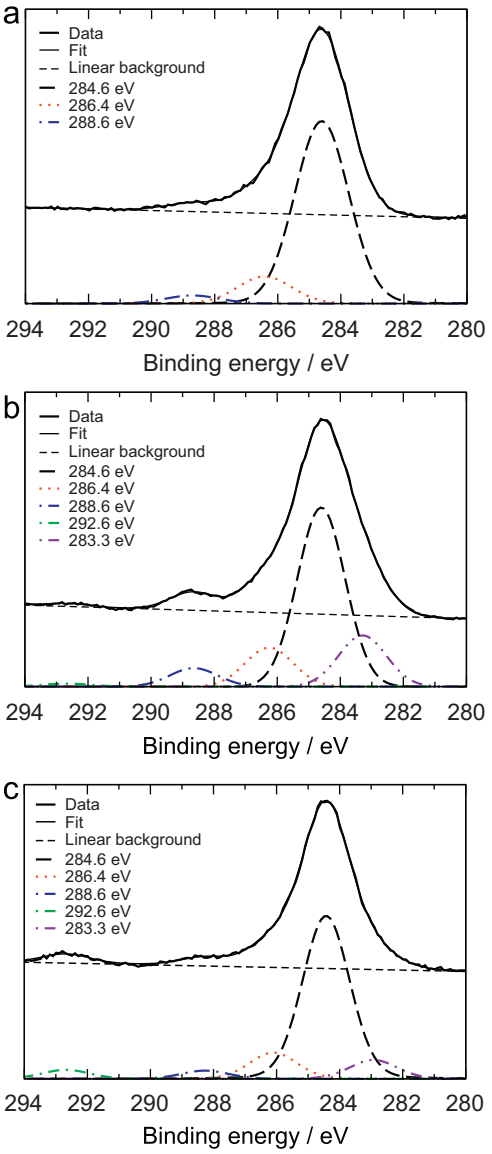

Fig. 9. Examples of curve fitting for the carbon 1*s* XPS peak for films with a (a) P:C ratio of 0, (b) P:C ratio of 0.22 and (c) P:C ratio of 0.46. (P:C ratio is the atomic ratio measured by XPS.)

associated with the peaks at binding energies of ~ 283.3 eV, ~ 288.6 eV and ~ 292.6 eV is shown as a function of composition in Fig. 10. The intensity of the peak at a binding energy of ~ 288.6 eV initially increases with increasing phosphorus content and then decreases, consistent with the qualitative observation (Fig. 6). The same trend is observed for the peak at a binding energy of ~ 283.3 eV. Therefore, these two peaks are likely to be associated with two different bonding environments for carbon found in a single type of structure. Based on computational results, both of these binding energies are consistent with those expected for β-InS-like phosphorus carbide structures.

The proportion of phosphorus associated with the two peaks attributed to P–C bonds (with binding energies of ~ 131.3 eV and ~ 133.7 eV) is shown as a function of phosphorus content in Fig. 11a. The proportion of the phosphorus with a binding energy of ~ 131.3 eV decreases as the phosphorus content increases. Assuming that the phosphorus with this binding energy is associated with P–C bonds found in the same phosphorus carbide structures that gives rise to the carbon 1*s* XPS signals at 288.6 eV and 283.3 eV, the proportion of carbon associated with these signals

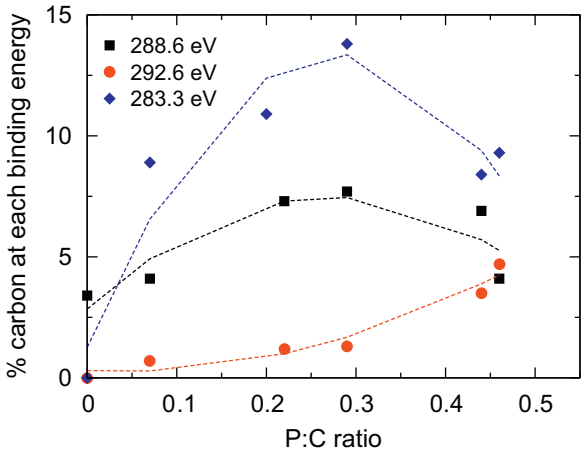

Fig. 10. Percentage of carbon associated with the peaks at binding energies of ~288.6 eV, ~292.6 eV and ~283.3 eV as a function of the P:C ratio. Percentage of carbon is taken neglecting carbon involved in C–O bonds. Dashed lines are quadratic fits of the data and serve to guide the eye.

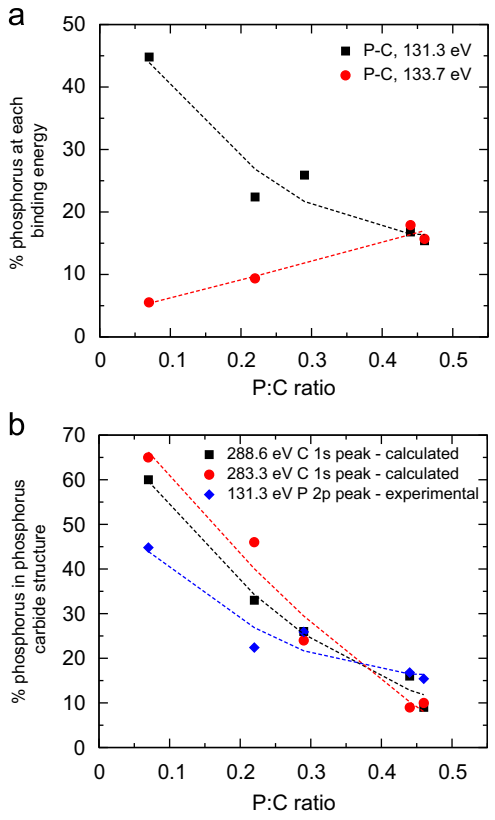

Fig. 11. (a) Percentage of phosphorus associated with the two XPS signals attributed to P–C bonds (corresponding to binding energies of ~131.3 eV and ~133.7 eV) as a function of the P:C ratio. Percentage of phosphorus is taken neglecting phosphorus involved in P–O bonds. (b) Percentage of phosphorus expected to be in phosphorus carbide structures of the same type that give rise to carbon 1*s* peaks at ~288.6 eV and ~283.3 eV, calculated from the amount of carbon that is associated with these two peaks. (In the case of the calculation based on the ~283.3 eV peak, it was necessary to divide by factor of two in order to achieve approximate quantitative agreement with the percentage of phosphorus associated with the XPS signal at ~131.3 eV. It should be noted that this factor of two is expected for a composition of PC_3, for which the structure is shown in Fig. 8, since there are twice as many carbon atoms in the bonding environment associated with the XPS signal at ~283.3 eV as phosphorus atoms in the bonding environment associated with the XPS signal at ~131.3 eV.) Dashed lines are quadratic fits of the data and serve to guide the eye.

can be used, along with the known composition of the samples, to calculate the proportion of the phosphorus expected to be associated with the same bonding environment. These calculated results are shown in Fig. 11b; there is very good agreement between the calculated value of the proportion of phosphorus expected to be involved in this bonding environment and the value determined by curve fitting of the phosphorus 2*p* peak. Hence, it is likely that the XPS signals at ~131.3 eV for phosphorus 2*p* and at 288.6 eV and 283.1 eV for carbon 1*s* are all associated with bonding environments found in the same structure. Furthermore, all three of these XPS signals are consistent with those expected for a β-InS-like structure. From the computational results, this is the type of structure that we predict to be preferred for a P:C ratio between 0.25 and 1, which overlaps the range found in our samples.

The films deposited by PLD contain regions of pure carbon and phosphorus, as indicated by XPS peaks assigned to P–P and C–C bonding and the presence of a strong peak attributed to sp^2 carbon bonding structures in the Raman spectra. However, there is also evidence that there are regions of the films with direct P–C bonding and hence regions where phosphorus carbide has formed. While the peaks in the XPS spectra assigned to P–C bonding are weak, and hence assignment of these peaks is difficult, there are two important factors that support the assignment of these peaks to P–C bonds. The first is that these assignments are consistent with previous reports of the binding energy of XPS peaks assigned to P–C bonds in phosphorus carbide materials [10,14,15]. The second important factor is the correlation between the phosphorus 2*p* and carbon 1*s* signals. Previous assignments of XPS peaks to P–C bonding have been based only on the phosphorus 2*p* region of the spectra. Correlation between the phosphorus 2*p* and carbon 1*s* XPS signals, as strong evidence of direct P–C bonding and the formation of phosphorus carbide structures, has not been reported previously. Furthermore, the detection of P_xC_y species in the SIMS spectra suggests that P–C bonds are indeed present.

3.3.4. Phosphorus-rich structures

The proportion of phosphorus associated with the XPS signal at ~133.7 eV increases as the phosphorus content increases (Fig. 11a), mirroring the trend seen for the carbon 1*s* signal at 292.6 eV (Fig. 10). Hence, it is likely that these two peaks correspond to the same type of structure. Furthermore, it is likely that they correspond to bonding environments in phosphorus-rich structures.

Our computational studies did not include highly phosphorus-rich compositions (>57 at%), so cannot assist here. Since the oxygen content increases with phosphorus content, the XPS peaks observed for samples with a high phosphorus content may be due to a phosphorus oxycarbide material, in which the XPS peak observed at a binding energy of ~133.7 eV is due to phosphorus in a high oxidation state [10].

3.4. Alternative assignments of XPS peaks

An alternative assignment for the carbon 1*s* signals at binding energies above that of sp^2 carbon (~288.6 eV and ~292.6 eV) is carboxylate and carbonate species [34,46]. Indeed, the presence of a small peak at ~288.6 eV for the samples containing no phosphorus (Fig. 10) suggests that there may be a small contribution of carboxylate and carbonate species to this peak.[3] However, the strong correlation between the intensity of the peaks observed for carbon 1*s* and those observed for phosphorus 2*p* peaks (*e.g.* the correlation between the intensity of the signals at ~288.6 eV for carbon 1*s* and at ~131.3 eV for phosphorus 2*p*, as demonstrated in Fig. 11, and also the correlation between the intensity of the signals at ~292.6 eV for carbon 1*s* and

[3] The presence of the peak at ~288.6 eV for samples with no phosphorus may simply be an artefact of the fitting; this peak is not seen for the samples containing no phosphorus if a Shirley background is used instead of a linear background.

at ~133.7 eV for phosphorus 2*p*) suggests that the assignment of these carbon 1*s* signals predominantly to bonds in P_xC_y structures is highly plausible. In addition, the peak at ~288.6 eV being due to carboxylate or carbonate species is inconsistent with the fact that the intensity of this peak starts to decrease when the P:C ratio exceeds ~0.3 (Fig. 10), given that the oxygen content of the films increases with phosphorus content (Fig. 2b). Also, results from SIMS analysis suggest that a large quantity of P_xC_y species are present but very little C_xO_y. Therefore, it seems unlikely that these signals are due exclusively to carboxylate and carbonate species (although, as noted above, the carbon 1*s* and phosphorus 2*p* peaks at high binding energies seen in samples with a relatively high phosphorus content could be due to phosphorus oxycarbide material). Another alternative assignment for the peak at ~292.6 eV is the π to π^* transition of graphite [47,48]. However, this peak is not seen in the samples that do not contain phosphorus so this assignment is unlikely.

3.5. Effect of substrate heating

The silicon substrate was heated (while still under vacuum in the deposition chamber) at 400 °C for 30 min after film deposition to determine the effect of heating on the composition and structure and specifically to determine if heating could promote crystallisation. However, it was found that heating leads to segregation of phosphorus and carbon. XPS results show an increase in the intensity of the carbon 1*s* signal at a binding energy of 284.6 eV after heating, while the peaks attributed to P–C bonding disappear (Fig. 12a). XPS also indicates that the phosphorus content is significantly reduced by the heat treatment (Fig. 12b) and the remaining phosphorus is mostly bonded to oxygen. This suggests that the phosphorus is volatile and not tightly bound to carbon. SIMS depth profiles suggest that this loss of phosphorus occurs mainly near the surface of the films. In support of this, measurement of the P:C ratio by energy-dispersive X-ray spectroscopy (EDXS), which detects the composition through the entire film depth rather than just near the surface as for XPS, indicates a smaller phosphorus loss than that indicated by XPS. Raman spectroscopy shows a significant increase in the intensity of the peak caused by sp^2 carbon with a shift to a higher wavenumber after heating (Fig. 12c). It is likely that this wavenumber shift corresponds to an increase in the intensity of the G component of this peak relative to the D component, as the extent of order in the sp^2 carbon structures increases and formation of graphite-like regions occurs with heating.

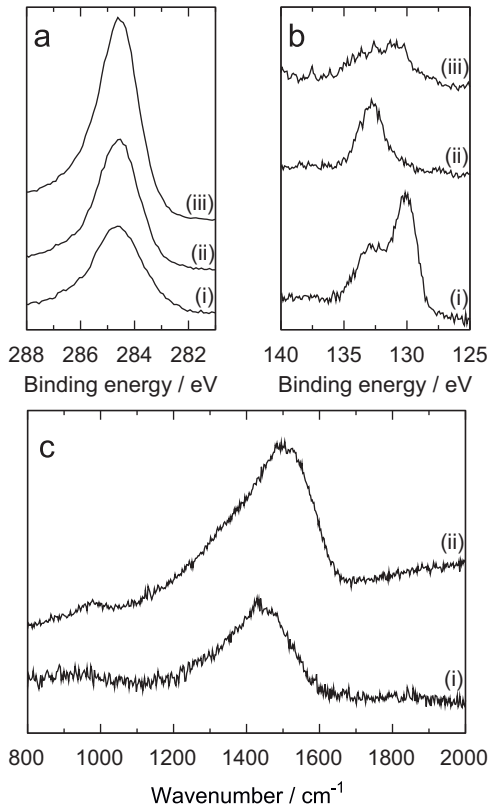

Fig. 12. (a) Carbon 1*s* XPS spectra of phosphorus–carbon films deposited from a target containing 28 at% with (i) no heat treatment, (ii) a heat treatment at 400 °C for 30 min after film deposition and (iii) deposited on a substrate heated to 400 °C; (b) as for (a), but phosphorus 2*p* XPS spectra; (c) Raman spectra of phosphorus–carbon films deposited from a target containing 28 at% with (i) no heat treatment and (ii) a heat treatment at 400 °C for 30 min. Composition is reported for the target, since the composition for films with and without heat treatments are different.

Depositing the film on a substrate maintained at a temperature of 400 °C results in a very low phosphorus content (as measured by XPS, Fig. 12b, SIMS and EDXS), while the XPS spectra suggest the presence of a large number of carbon-carbon bonds (Fig. 12a).

Thus, we conclude that heating the substrate does not promote formation of crystalline phosphorus carbide, consistent with the computational results which indicate that crystalline phosphorus carbide is thermodynamically unstable relative to graphite and elemental phosphorus at low pressures [6].

4. Conclusions

Amorphous phosphorus–carbon films with a range of compositions have been synthesised by pulsed laser deposition. While crystalline material has not been formed and the films contain regions of both pure carbon and phosphorus, we have found strong evidence of regions with direct P–C bonding and hence phosphorus carbide formation. Good agreement was found between the local bonding environments found in these phosphorus carbide regions and those predicted in computational work. In particular, the local bonding environments of both carbon and phosphorus determined from XPS analysis are consistent with the β-InS-like structures that have been predicted to be low in energy for phosphorus carbide. As it has not been possible to form crystalline phosphorus carbide by pulsed laser deposition, even with the application of heat treatments, further work will include studies of the high pressure crystallisation behaviour of phosphorus carbide, since the thermodynamic stability of these materials is expected to increase under hydrostatic pressure. Since phosphorus carbide is expected to be a semiconductor, analysis of the valence bands of the deposited films by ultraviolet photoelectron spectroscopy would be highly informative but is beyond the scope of the current work.

Acknowledgments

J.N.H. gratefully acknowledges funding from the Ramsay Memorial Fellowships Trust and the Royal Society.

Appendix A. Supplementary material

Supplementary data associated with this article can be found in the online version, at http://dx.doi.org/10.1016/j.jssc.2012.11.008.

References

[1] A.Y. Liu, M.L. Cohen, Science 245 (1989) 841–842.
[2] L. Yang, P.W. May, L. Yin, R. Brown, T.B. Scott, Chem. Mater. 18 (2006) 5058–5064.

[3] X. Yan, T. Xu, G. Chen, S. Yang, H. Liu, Q. Xue, J. Phys. D: Appl. Phys. 37 (2004) 907–913.
[4] I. Widlow, Y.W. Chung, Int. Mater. Rev. 47 (2002) 153–167.
[5] J.N. Hart, F. Claeyssens, N.L. Allan, P.W. May, Phys. Rev. B 80 (2009) 174111.
[6] F. Claeyssens, J.N. Hart, N.L. Allan, J.M. Oliva, Phys. Rev. B 79 (2009) 134115.
[7] F. Claeyssens, J.M. Oliva, P.W. May, N.L. Allan, Int. J. Quantum Chem. 95 (2003) 546–553.
[8] F. Claeyssens, G.M. Fuge, N.L. Allan, P.W. May, M.N.R. Ashfold, Dalton Trans. (2004) 3085–3092.
[9] F. Claeyssens, N.L. Allan, P.W. May, P. Ordejon, J.M. Oliva, Chem. Commun. (2002) 2494–2495.
[10] J. Gorham, J. Torres, G. Wolfe, A. d'Agostino, D.H. Fairbrother, J. Phys. Chem. B 109 (2005) 20379–20386.
[11] S.R.J. Pearce, J. Filik, P.W. May, R.K. Wild, K.R. Hallam, P.J. Heard, Diamond Relat. Mater. 12 (2003) 979–982.
[12] S.R.J. Pearce, P.W. May, R.K. Wild, K.R. Hallam, P.J. Heard, Diamond Relat. Mater. 11 (2002) 1041–1046.
[13] M.T. Kuo, P.W. May, A. Gunn, M.N.R. Ashfold, R.K. Wild, Diamond Relat. Mater. 9 (2000) 1222–1227.
[14] A. Liu, J. Zhu, J. Han, H. Wu, W. Gao, Electroanalysis 19 (2007) 1773–1778.
[15] A. Furlan, G.K. Gueorguiev, Z. Czigány, H. Hogberg, S. Braun, S. Stafström, L. Hultman, Phys. Status Solidi Rapid Res. Lett. 2 (2008) 191–193.
[16] M.M. Golzan, D.R. McKenzie, D.J. Miller, S.J. Collocott, G.A.J. Amaratunga, Diamond Relat. Mater. 4 (1995) 912–916.
[17] A. Liu, J. Zhu, M. Tan, X. Han, W. Chen, J. Han, Phosphorus Sulfur Silicon Relat. Elem. 183 (2008) 657–664.
[18] G.K. Gueorguiev, A. Furlan, H. Hogberg, S. Stafström, L. Hultman, Chem. Phys. Lett. 426 (2006) 374–379.
[19] A. Furlan, G.K. Gueorguiev, H. Hogberg, S. Stafström, L. Hultman, Thin Solid Films 515 (2006) 1028–1032.
[20] E. Broitman, A. Furlan, G.K. Gueorguiev, Z. Czigány, A.M. Tarditi, A.J. Gellman, S. Stafström, L. Hultman, Surf. Coat. Technol. 204 (2009) 1035–1039.
[21] K. Momma, F. Izumi, J. Appl. Crystallogr. 41 (2008) 653–658.
[22] S.C.H. Kwok, W. Jin, P.K. Chu, Diamond Relat. Mater. 14 (2005) 78–85.
[23] S.C.H. Kwok, G. Wan, J.P.Y. Ho, P.K. Chu, D.R. McKenzie, M.M.M. Bilek, New Diam. Front. C. Tec. 16 (2006) 39–48.
[24] S.C.H. Kwok, P.C.T. Ha, D.R. McKenzie, M.M.M. Bilek, P.K. Chu, Diamond Relat. Mater. 15 (2006) 893–897.
[25] S. Kelly, E.M. Regan, J.B. Uney, A.D. Dick, J.P. McGeehan, E.J. Mayer, F. Claeyssens, Biomaterials 29 (2008) 2573–2580.
[26] E.M. Regan, J.B. Uney, A.D. Dick, Y.W. Zhang, J. Nunez-Yanez, J.P. McGeehan, F. Claeyssens, S. Kelly, Biomaterials 31 (2010) 207–215.
[27] M. Wojdyr, J. Appl. Crystallogr. 43 (2010) 1126–1128.
[28] P. Mérel, M. Tabbal, M. Chaker, S. Moisa, J. Margot, Appl. Surf. Sci. 136 (1998) 105–110.
[29] P.A. Brühwiler, A.J. Maxwell, C. Puglia, A. Nilsson, S. Andersson, N. Martensson, Phys. Rev. Lett. 74 (1995) 614–617.
[30] J. Díaz, G. Paolicelli, S. Ferrer, F. Comin, Phys. Rev. B 54 (1996) 8064–8069.
[31] F. Sette, G.K. Wertheim, Y. Ma, G. Meigs, S. Modesti, C.T. Chen, Phys. Rev. B 41 (1990) 9766–9770.
[32] A.C. Ferrari, J. Robertson, Phys. Rev. B 61 (2000) 14095–14107.
[33] C.E. Myers, H.F. Franzen, J.W. Anderegg, Inorg. Chem. 24 (1985) 1822–1824.
[34] NIST X-ray Photoelectron Spectroscopy Database, Version 3.5, National Institute of Standards and Technology, Gaithersburg, 2003.
[35] R. Dovesi, V.R. Saunders, C. Roetti, R. Orlando, C.M. Zicovich-Wilson, F. Pascale, B. Civalleri, K. Doll, N.M. Harrison, I.J. Bush, P. D'Arco, M. Llunell, CRYSTAL06 Users Manual, University of Torino, Torino, Italy, 2006.
[36] R. Dovesi, V.R. Saunders, C. Roetti, R. Orlando, C.M. Zicovich-Wilson, F. Pascale, B. Civalleri, K. Doll, N.M. Harrison, I.J. Bush, P. D'Arco, M. Llunell, CRYSTAL09 Users Manual, University of Torino, Torino, Italy, 2009.
[37] R. Dovesi, R. Orlando, B. Civalleri, C. Roetti, V.R. Saunders, C.M. Zicovich-Wilson, Z. Kristallogr. 220 (2005) 571–573.
[38] A.D. Becke, J. Chem. Phys. 98 (1993) 5648–5652.
[39] C.T. Lee, W.T. Yang, R.G. Parr, Phys. Rev. B 37 (1988) 785–789.
[40] R. Orlando, R. Dovesi, C. Roetti, V.R. Saunders, J. Phys.: Condens. Matter 2 (1990) 7769–7789.
[41] R. Nada, C.R.A. Catlow, R. Dovesi, C. Pisani, Phys. Chem. Miner. 17 (1990) 353–362.
[42] R. Nada, J.B. Nicholas, M.I. McCarthy, A.C. Hess, Int. J. Quantum Chem. 60 (1996) 809–820.
[43] A. Lichanot, M. Causà, J. Phys.: Condens. Matter 9 (1997) 3139–3149.
[44] E. Ruiz, M. Llunell, P. Alemany, J. Solid State Chem. 176 (2003) 400–411.
[45] C. Adamo, V. Barone, J. Chem. Phys. 110 (1999) 6158–6170.
[46] R.I.R. Blyth, H. Buqa, F.P. Netzer, M.G. Ramsey, J.O. Besenhard, P. Golob, M. Winter, Appl. Surf. Sci. 167 (2000) 99–106.
[47] F.R. McFeely, S.P. Kowalczy, L. Ley, R.G. Cavell, R.A. Pollak, D.A. Shirley, Phys. Rev. B 9 (1974) 5268–5278.
[48] V.S. Smentkowski, H. Jansch, M.A. Henderson, J.T. Yates, Surf. Sci. 330 (1995) 207–226.